Available online at www.sciencedirect.com
ScienceDirect
Trans. Nonferrous Met. Soc. China 27(2017) 599−607
Transactions of Nonferrous Metals Society of China
www.tnmsc.cn

Morphological evolution and growth kinetics of Kirkendall voids in binary alloy system during deformation process—Phase field crystal simulation study

Wen-jing MA, Chang-bo KE, Shui-bao LIANG, Min-bo ZHOU, Xin-ping ZHANG

School of Materials Science and Engineering, South China University of Technology, Guangzhou 510640, China

Received 12 May 2016; accepted 18 September 2016

Abstract: The formation and growth of Kirkendall voids in a binary alloy system during deformation process were investigated by phase field crystal model. The simulation results show that Kirkendall voids nucleate preferentially at the interface, and the average size of the voids increases with both the time and strain rate. There is an obvious coalescence of the voids at a large strain rate when the deformation is applied along the interface under both constant and cyclic strain rate conditions. For the cyclic strain rate applied along the interface, the growth exponent of Kirkendall voids increases with increasing the strain rate when the strain rate is larger than 1.0×10^{-6}, while it increases initially and then decreases when the strain rate is smaller than 9.0×10^{-7}. The growth exponent of Kirkendall voids increases initially and then decreases gradually with increasing the length of cyclic period under a square-wave form constant strain rate.

Key words: Kirkendall void; binary alloy; phase field crystal method; growth exponent; deformation

1 Introduction

Kirkendall voids exist widely in solders, films and nanometer materials. Notably, with the development of electronic products towards further miniaturization, multifunction and high-reliability, the packing density has been increasing and the dimension of solder interconnects (joints) has been scaling down [1−4], and the existence of Kirkendall voids may increase the potential for brittle interfacial fracture of solder joints and reduce the thermal conductivity [5−7]. Massive Kirkendall voids often appear at the interface of solder joints and can be affected by deformation during the solid-state thermal aging and electromigration process [8−10]. In particular, the deformation and stress caused by the electromigration may accelerate (or decelerate) the growth of voids at the cathode (or anode) [11]. In addition, constant creep deformation of solder joints usually occurs in constant power operation of electronic components. But the power is often fluctuated during the actual application, which produces thermal cycling and leads to a cyclic creep deformation. The presence of the deformation affects not only the mechanical property and crystal structure of the joint materials, but also the nucleation and growth of Kirkendall voids in solder joints [12].

Although Kirkendall voids can be clearly observed in experiments and there is a relation between the failure of solder joints and Kirkendall voids [13−18], it is still very difficult to reveal the formation and evolution mechanism of Kirkendall voids which form quickly at the interface of microscale solder joints. In general, there are various kinds of deformation occurring in the solder joints, such as constant deformation and cyclic deformation. Thus, it is necessary to introduce reliable models and numerical methods to describe the nucleation and growth of Kirkendall voids during deformation process. Phase field crystal (PFC) method has shown the great potential for studying the formation and growth process of Kirkendall voids. Furthermore, the PFC method has emerged as an attractive computational approach to tackle interfacial problems [19], especially it has the advantage to study the interfacial reaction and microstructure evolution in the atomic scale.

In this study, the formation and growth of Kirkendall voids during deformation process in a binary alloy system, which is equivalent to a binary soldering

Foundation item: Projects (51275178, 51405162, 51205135) supported by the National Natural Science Foundation of China; Projects (20110172110003, 20130172120055) supported by the Doctoral Program of Higher Education of China
Corresponding author: Xin-ping ZHANG; Tel: +86-20-22236396; Fax: +86-20-22236393; E-mail: mexzhang@scut.edu.cn
DOI: 10.1016/S1003-6326(17)60067-0

system consisting of a solder and a substrate, were investigated by means of PFC modeling. The strain rate was employed to describe the deformation. Since a constant strain rate was applied to all atoms, a constant deformation was obtained. Other forms of deformation can be obtained by the similar ways. The influence of various strain rates (including the constant strain rate and cyclic strain rate) and the length of cycle period of the cyclic strain rate on the evolution and growth kinetics of Kirkendall voids were systematically examined.

2 Model

2.1 Numerical model of binary alloy system

In this study, we consider a binary alloy consisting of A and B atoms. The free energy functional in dimensionless form can be written as [19]

$$F=\int \mathrm{d}\vec{x}[\frac{n}{2}\Lambda^0 n-\frac{m}{3}n^3+\frac{\nu}{4}n^4+\gamma\psi+\frac{\omega}{2}\psi^2+\frac{u}{4}\psi^4+\frac{K}{2}|\vec{\nabla}\psi|^2] \tag{1}$$

$$\Lambda^0\equiv(B_0^{\mathrm{l}}-B_0^{\mathrm{x}})+B_2^{\mathrm{l}}\psi^2+B_0^{\mathrm{x}}(1+\nabla^2)^2 \tag{2}$$

where B_0^{l} describes the dimensionless bulk modulus of the liquid phase; B_0^{x} describes the dimensionless bulk modulus of the crystalline phase; B_2^{l} is related to phase diagram, n describes the number density; ψ describes the concentration; m and ν characterize the fluctuation amplitude; ω is related to the difference between interspecies bond energy and self-bond energy; u and γ describe atomic interactions in the system; K is related to the gradient energy coefficient for the concentration field. More convenient equations of motion for the dimensionless atomic number density of each species are incorporated to study the Kirkendall effect [20].

The motion equations can be written as [20]

$$\frac{\partial n_{\mathrm{A}}}{\partial t}=M_{\mathrm{A}}\nabla^2\frac{\delta F}{\delta n_{\mathrm{A}}}=M_{\mathrm{A}}\nabla^2[\Lambda^0 n-mn^2+\nu n^3+(\omega+B_2^{\mathrm{l}}n^2)\psi+u\psi^3-K\nabla^2\psi] \tag{3}$$

$$\frac{\partial n_{\mathrm{B}}}{\partial t}=M_{\mathrm{B}}\nabla^2\frac{\delta F}{\delta n_{\mathrm{B}}}=M_{\mathrm{B}}\nabla^2[\Lambda^0 n-mn^2+\nu n^3-(\omega+B_2^{\mathrm{l}}n^2)\psi-u\psi^3+K\nabla^2\psi] \tag{4}$$

where M_{A} is the dimensionless mobility of A atom; M_{B} is the dimensionless mobility of B atom; ρ_{A}, ρ_{B} and ρ_{l} are the atomic number densities of A atom, B atom and a supercooled liquid phase, respectively; n_{A} and n_{B} are the dimensionless atomic number densities of A and B atoms respectively; $n_{\mathrm{A}}\equiv(n+\psi)/2=\rho_{\mathrm{A}}/\rho_{\mathrm{l}}$ and $n_{\mathrm{B}}\equiv(n-\psi)/2=\rho_{\mathrm{B}}/\rho_{\mathrm{l}}$.

The free energy can be equivalently defined in terms of density (n) and concentration (ψ), which allows the dynamic equations to be rewritten as follows:

$$\frac{\partial n}{\partial t}=(M_{\mathrm{A}}+M_{\mathrm{B}})\nabla^2(\Lambda^0 n-mn^2+\nu n^3)+(M_{\mathrm{A}}-M_{\mathrm{B}})\nabla^2[(\omega+B_2^{\mathrm{l}}n^2)\psi+u\psi^3]+(M_{\mathrm{B}}-M_{\mathrm{A}})\nabla^2K\nabla^2\psi \tag{5}$$

$$\frac{\partial \psi}{\partial t}=(M_{\mathrm{A}}-M_{\mathrm{B}})\nabla^2(\Lambda^0 n-mn^2+\nu n^3)+(M_{\mathrm{A}}+M_{\mathrm{B}})\nabla^2[(\omega+B_2^{\mathrm{l}}n^2)\psi+u\psi^3]-(M_{\mathrm{A}}+M_{\mathrm{B}})\nabla^2K\nabla^2\psi \tag{6}$$

A single-mode approximation for the total density, n, was used [19]:

$$n(x,y,t=0)=\overline{n}+A[\cos(2q_y y/2)-\cos(q_x x)\cos(q_y y)] \tag{7}$$

where $q_x=2\pi/a$, a=6.927, a describes the equilibrium lattice constant, $q_y=q_x/\sqrt{3}$; A is a constant, A=0.5; $\overline{n}$ describes the number density difference and $\overline{n}$ =−0.1503.

The thermal fluctuation noise term affecting the evolution of the system has been neglected in this simulation. Equations (5) and (6) are solved numerically by using a simple Euler algorithm for the time derivative, and the usual spherical Laplacian approximation is adopted for all spatial gradients. In the simulation, the dimensionless time step is used, Δt=0.01. The configuration and dimensions of the simulation system are shown in Fig. 1, where the dimensions of the simulation region are set to be 512Δx along the x-axis direction (i.e., along the interface) and 200Δy along the y-axis direction (i.e., vertical to the interface), and $\Delta x=\Delta y$=0.989634. The boundary conditions ψ and n are periodic along the x-axis, while the Neumann type boundary conditions are adopted at the bottom (1Δy) and top surface (200Δy). The α phase layer (A atom-rich phase), L phase layer (Supercooled liquid phase) and β phase layer (B atom-rich phase) are positioned in horizontal layers from the bottom of the domain to the domain top; the α phase layer is set between 1Δy and 98Δy, the L phase layer is set between 99Δy and 102Δy, and the rest of the region is pre-occupied by the β phase.

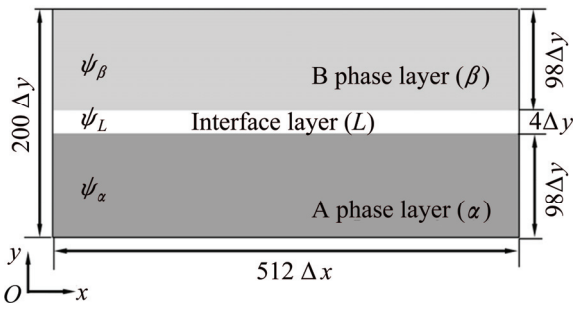

Fig. 1 Configuration and dimensions of computational domain

In the early stage of evolution process, the liquid layer solidifies and naturally forms an interface between the two phase layers, and atoms on both sides of the interface layer continuously assimilate the interface to form an atomic mismatch region. Kirkendall voids nucleation and growth occur in the atomic mismatch region at the interface. The atomic mismatch region at the interface can be considered as the premelting and melting grain boundary. According to the previous studies [19−21], when the temperature infinitely approaches the critical melting temperature of an alloy, the atomic mismatch regions relate to the wetting temperature, the melting temperature and interface misorientation angle. With referring to the previous research on the small interface misorientation angle about Kirkendall voids [20], an interface misorientation angle of 4.8° is chosen. In this simulation work, the initial concentration for each phase is set as follows: ψ_L=0, ψ_α=−0.2 and ψ_β=0.2 according to the model proposed by ELDER et al [20]. The positive concentration indicates the faster diffuser while the slower diffuser is represented with a negative value. The parameters used in the simulation are listed in Table 1.

Table 1 Material parameters used in simulation [20]

B_0^l	B_2^l	B^x	K	m	v	ω	u
0.7	−1.8	1	4.0	0.6	1.0	1.0	4.0

2.2 Deformation simulation

A numerical technique was used to perform the PFC method deformation simulation. In the simulation, deformation volume is kept constant to ensure that the simulation can reveal the appropriate deformation behavior of metallic materials like solders. Figure 2 shows the numerical technique for analyzing the deformation by the PFC simulation in two dimensions. The increment of each time step in the x-axis direction is described as $d = \dot{\varepsilon}\Delta x\Delta t = \varepsilon\Delta x/N$. Here, Δx is the initial grid size, $\dot{\varepsilon}$ is the dimensionless strain rate, ε is the strain and N is the total time step. After running the simulation for one time step, the size is increased by $\Delta x'=\Delta x+Nd$ and $\Delta y'=(\Delta x\Delta y)/\Delta x'$ in the x and y directions, respectively, and the increment of each time step is a constant [22].

In Fig. 2, S represents the area of the simulation system, S_1 and S_2 are the grid sizes of the initial and deformed areas, respectively; Δx and Δy are the initial grid sizes in the x and y directions, respectively; $\Delta x'$ and $\Delta y'$ are the deformed grid sizes in the x and y directions, respectively. Equations (5) and (6) ensure that the deformation volume is a constant. The conventional spherical Laplacian approximation, as described in Eq. (8), was used in the case of equal grid size [23,24], while the modified spherical Laplacian approximation, as shown in Eq. (9), was employed in the case of unequal grid size:

$$\nabla^2 f_{i,j} = \frac{1}{(\Delta x)^2}[\frac{1}{2}(f_{i+1,j}+f_{i-1,j}+f_{i,j+1}+f_{i,j-1})+ \frac{1}{4}(f_{i+1,j+1}+f_{i-1,j+1}+f_{i+1,j-1}+f_{i-1,j-1})-3f_{i,j}] \quad (8)$$

$$\nabla^2 f_{i,j} = \frac{\partial^2 f_{i,j}}{\partial x^2}+\frac{\partial^2 f_{i,j}}{\partial y^2} = \frac{1}{(\Delta x')^2}\cdot[\frac{1}{8}(f_{i+1,j+1}+ f_{i-1,j+1}+f_{i+1,j-1}+f_{i-1,j-1})+\frac{3}{4}(f_{i-1,j}+f_{i+1,j})- \frac{1}{4}(f_{i,j+1}+f_{i,j-1})-\frac{3}{2}f_{i,j}]+ \frac{1}{(\Delta y')^2}[\frac{1}{8}(f_{i+1,j+1}+ f_{i-1,j+1}+f_{i+1,j-1}+f_{i-1,j-1})+\frac{3}{4}(f_{i,j+1}+f_{i,j-1})- \frac{1}{4}(f_{i+1,j}+f_{i-1,j})-\frac{3}{2}f_{i,j}] \quad (9)$$

Experimental observations reported in a previous study [18] indicated that the strain rate is related to the effective stress σ, material constant $\dot{\varepsilon}_c$ and yield stress

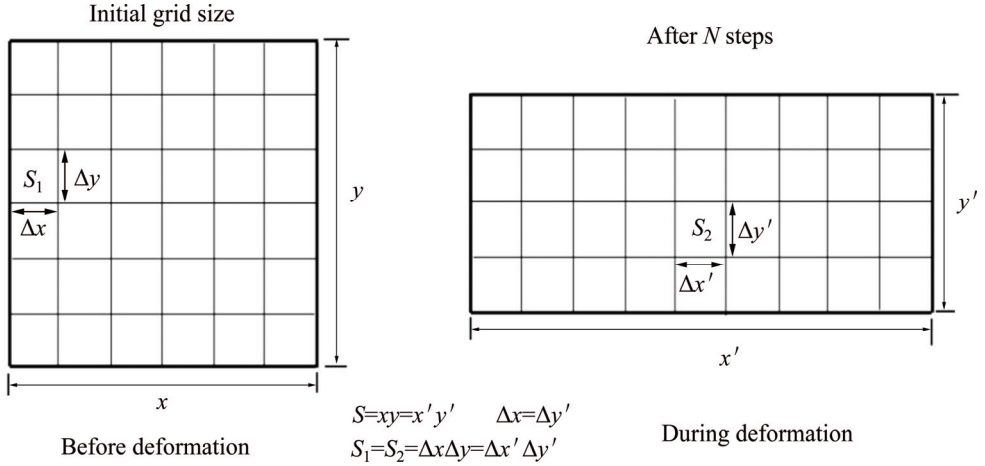

Fig. 2 Two-dimensional schematic configuration of tensile deformation simulation by PFC

σ_0. The dimensionless effective stress σ' at each time step is calculated by $\sigma'=\Delta f/\Delta\varepsilon$, where Δf is the change in free energy density, $\Delta\varepsilon$ is the strain increment during the time step Δt. Based on the experimental study on the formation behavior of IMC layer [18], the value of the typical strain rate is in the range of 10^{-5}–10^{-4}. In this simulation, the dimensionless strain rate $\dot{\varepsilon}$ is set to 1.0×10^{-8}–9.0×10^{-6}.

In this study, three different conditions are considered, as shown in Fig. 3. 1) Deformation with a constant strain rate ($\dot{\varepsilon}=1.0\times10^{-6}$–$9.0\times10^{-6}$) is applied along the interface (i.e., in the x-axis direction), as shown in Fig. 3(a); 2) Deformation with an alternating tensile-compressive square-wave form strain rate is applied along the interface; in this case, a constant strain rate ($\dot{\varepsilon}=1.0\times10^{-8}$–$9.0\times10^{-6}$) is applied during the first half cycle and the same constant strain rate in the opposite direction during the second half cycle, as shown in Figs. 3(b) and (c); 3) Deformation with a square-wave form constant strain rate ($\dot{\varepsilon}=6.0\times10^{-6}$) is applied along the interface, while varying the length of the cyclic (or period), as shown in Figs. 3(b) and (d). It should be noted that the length of the cyclic period in Figs. 3(b) and (c) is remained constant (T_L), while Fig. 3(d) shows a length of the cyclic period for $2T_L$.

3 Results and discussion

3.1 Evolution of Kirkendall voids under different constant strain rates

In simulations, deformations with three different constant strain rates, i.e., $\dot{\varepsilon}=6.0\times10^{-6}$, 3.0×10^{-6} and 1.0×10^{-6}, are applied along the interface, as shown in Fig. 3(a). The morphological evolution of Kirkendall voids is shown in Fig. 4. Clearly, with increasing t from 0 to 1.0×10^5, atoms on both sides of the interface layer continuously assimilate the interface to form an atomic mismatch region, as shown in Figs. 4(a_1), (b_1) and (c_1). The atomic mismatch region at the interface promotes the nucleation of Kirkendall voids by reducing the free energy barrier via decreasing the interface energy [11]. The atomic mismatched regions play a role in pinning

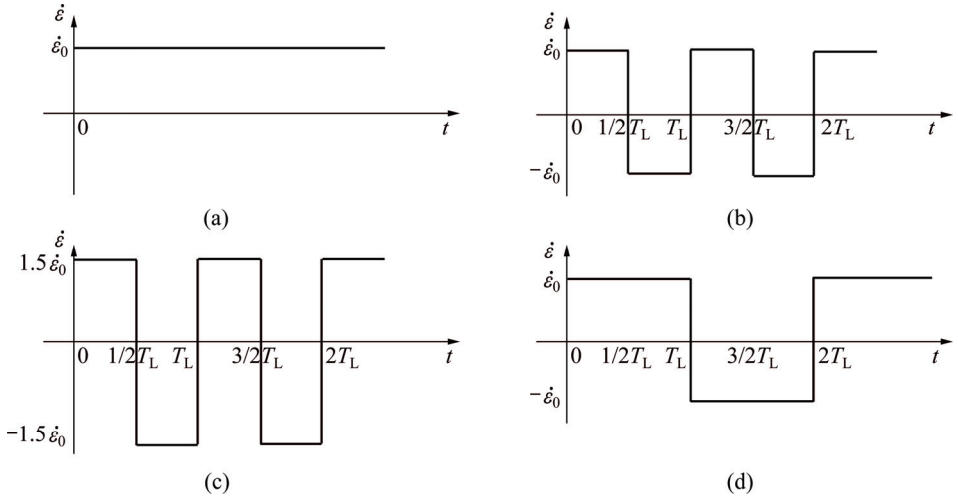

Fig. 3 Schematic of different loading conditions in deformation simulation: (a) Constant strain rate; (b) Square-wave form strain rate with low amplitude of $\dot{\varepsilon}_0$; (c) Square-wave form strain rate with increased amplitude of 1.5 $\dot{\varepsilon}_0$; (d) Square-wave form strain rate with large length of cyclic period for $2T_L$

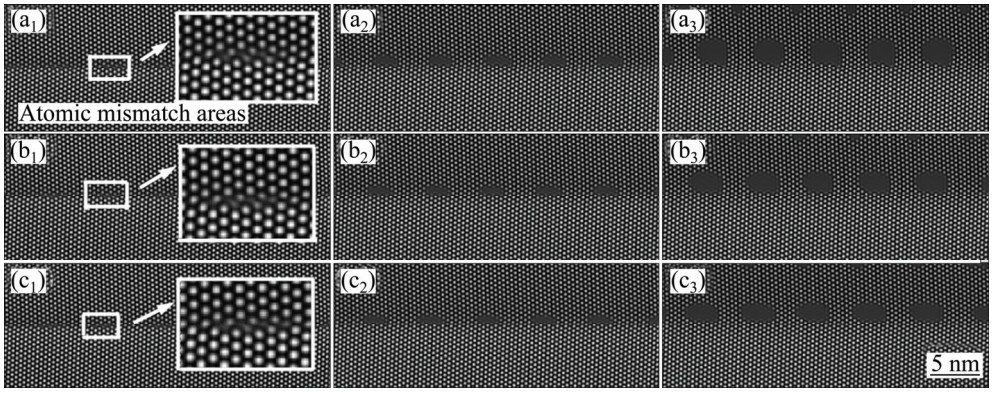

Fig. 4 Morphological evolution of Kirkendall voids with different constant strain rates of $\dot{\varepsilon}=6.0\times10^{-6}$ (a_1–a_3), $\dot{\varepsilon}=3.0\times10^{-6}$ (b_1–b_3), $\dot{\varepsilon}=1.0\times10^{-6}$ (c_1–c_3), and different time steps of t=1.0×10^5 (a_1–c_1), t=3.0×10^5 (a_2–c_2) and t=7.0×10^5 (a_3–c_3)

vacancy sinks, which cause the supersaturation of vacancy concentration. Kirkendall voids could grow towards the vacancy concentration supersaturation regions easily. Thus, Kirkendall voids nucleate preferentially at the interface. The size of Kirkendall voids increases with both the time and strain rate, and the coalescence of the voids can be observed obviously in the later stage of the evolution process. The larger the strain rate is, the greater the deformation is in the same time, and the more the atomic mismatch regions distribute on both upper and lower sides along the interface direction. These atomic mismatch regions can cause a higher growth rate of the Kirkendall voids along the vertical direction than along the horizontal direction. With decreasing the strain rate, the growth mode (or direction) of Kirkendall voids changes from the direction perpendicular to the interface to the direction parallel to the interface.

The diffusion-controlled growth of Kirkendall voids can be described by an exponential function [25]:

$$Y = K_t t^{n_y} \tag{10}$$

$$Y = \frac{1}{2}\left(\bar{D}_{\mathrm{L}} + \bar{D}_{\mathrm{H}}\right) \tag{11}$$

where Y is the average size of Kirkendall voids, t is the time step, n_y is the growth exponent, K_t is a constant, $\bar{D}_{\mathrm{L}}$ is the average value of the length dimensions as the average size of the voids, $\bar{D}_{\mathrm{H}}$ is the average value of the height dimensions as the average size of the voids.

The average size of Kirkendall voids changing with time under different strain rates and the growth exponent of Kirkendall voids versus level of strain rate are shown in Fig. 5. It is clear that the average size of Kirkendall voids increases with both the time and strain rate, as shown in Fig. 5(a). This is consistent with the results reported in Refs. [11,26]. Further, the growth exponent of Kirkendall voids under different values of $\dot{\varepsilon}$, from 1.0×10^{-6} to 9.0×10^{-6}, also increases with increasing the strain rate, as shown in Fig. 5(b). According to the classical theory of transformation in metals and alloys [27], the grain boundary nucleation after saturation occurs when the growth exponent is less than 1, while the grain edge nucleation after saturation takes place with a growth exponent between 1 and 2. The values of the growth exponent, which lie in the range of 0.585−0.788, indicate that the nucleation of Kirkendall voids occurs at the interface. Thus, in this simulation, the change in the strain rate shows no significant influence on the nucleation site of the voids.

3.2 Evolution of Kirkendall voids under different cyclic strain rates

For solder joints under actual service conditions, the deformation is often generated by the way of periodic cycle acting on the joints. The cyclic deformation often occurs under thermal cycling and electromigration circumstance as reported in Ref. [11].

Figure 6 shows the morphological evolution of Kirkendall voids under the loading condition shown in Figs. 3(b) and (c) with three different cyclic strain rates of 6.0×10^{-6}, 3.0×10^{-6} and 6.0×10^{-7} for different time elapsed from 1.0×10^{5} to 3.0×10^{5} and then to 7.0×10^{5}. It can be seen clearly that Kirkendall voids nucleate preferentially at the interface and grow parallel to the interface, and the size of the voids increases with the time. When the strain rate is large enough ($\dot{\varepsilon}\geq7.0\times10^{-6}$), the coalescence of the voids can be observed in the later stage of the evolution process. The size of the voids increases with increasing strain rate. Further, with increasing t from 0 to 1.0×10^{5}, atoms on both sides of the interface layer continuously assimilate the interface to form an atomic mismatch region at the interface, which results in the enhancement of the nucleation of Kirkendall voids by reducing the interface energy, as shown in Figs. 6(a_1), (b_1) and (c_1).

The average size of Kirkendall voids versus evolutionary time under different cyclic strain rates and the growth exponent of Kirkendall voids at different strain rates are shown in Fig. 7. It is clear that the

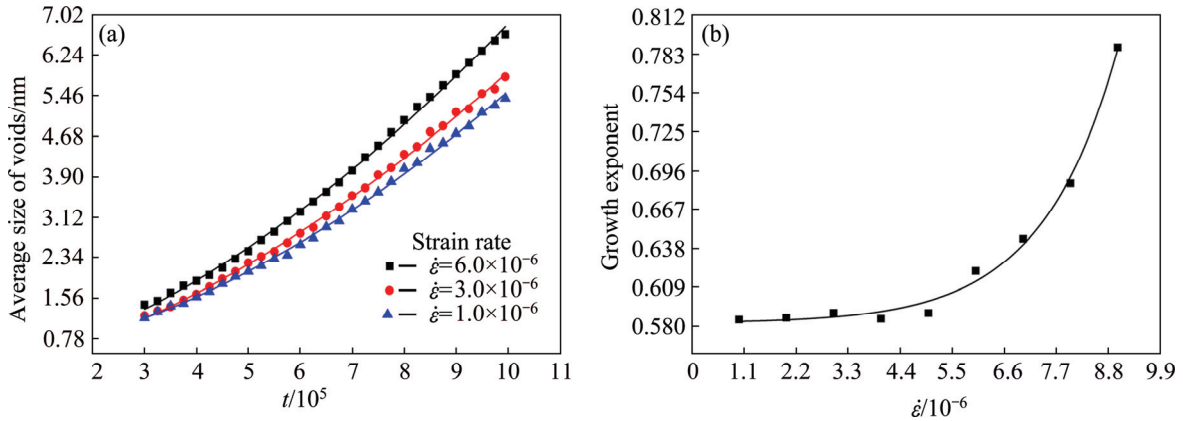

Fig. 5 Average size of Kirkendall voids vs time at different strain rates (a) and growth exponents of Kirkendall voids vs level of strain rate (b)

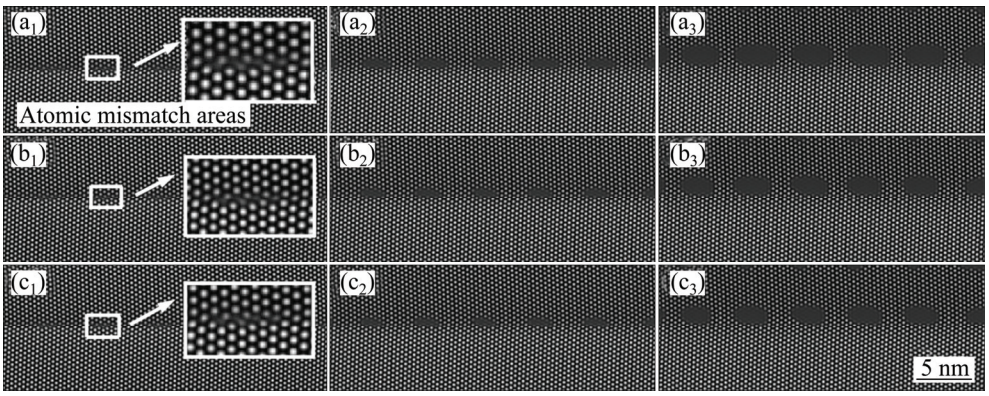

Fig. 6 Morphological evolution of Kirkendall voids under different cyclic strain rates of $\dot{\varepsilon}=6.0\times10^{-6}$ (a_1−a_3), $\dot{\varepsilon}=3.0\times10^{-6}$ (b_1−b_3), $\dot{\varepsilon}=6.0\times10^{-7}$ (c_1−c_3), and different time steps of $t=1.0\times10^5$ (a_1−c_1), $t=3.0\times10^5$ (a_2−c_2) and $t=7.0\times10^5$ (a_3−c_3)

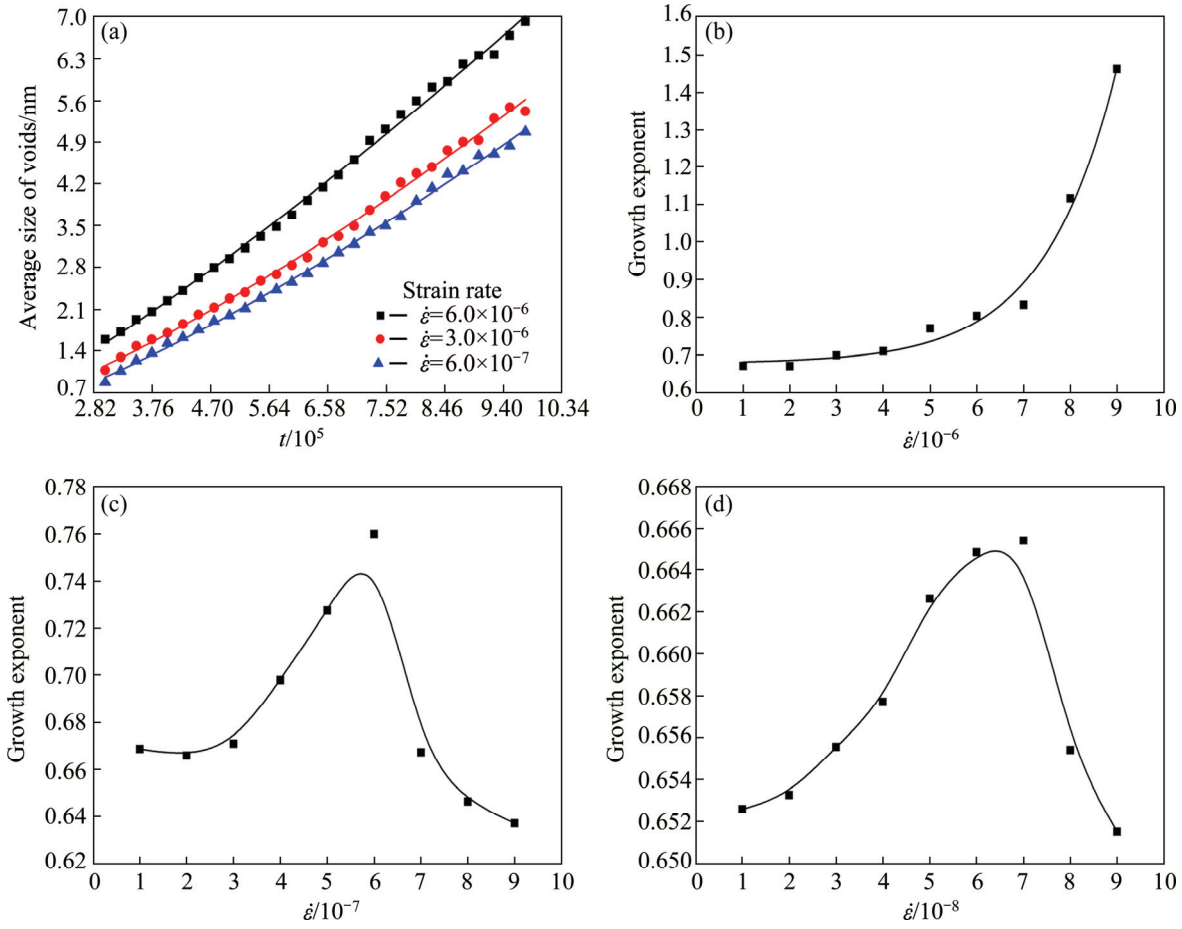

Fig. 7 Average size of Kirkendall voids vs time under different cyclic strain rates (a) and growth exponent of Kirkendall voids under different strain rate ranges of $\dot{\varepsilon}=1.0\times10^{-6}$–$9.0\times10^{-6}$ (b), $\dot{\varepsilon}=1.0\times10^{-7}$–$9.0\times10^{-7}$ (c) and $\dot{\varepsilon}=1.0\times10^{-8}$–$9.0\times10^{-8}$ (d)

average size of Kirkendall voids increases with increasing both of evolutionary time and strain rate, as shown in Fig. 7(a), which is in good coincidence with the results of the constitutive model simulation [18]. The values of the growth exponent of Kirkendall voids with the same cyclic period while in different strain rate ranges of 1.0×10^{-6} to 9.0×10^{-6}, 1.0×10^{-7} to 9.0×10^{-7} and 1.0×10^{-8} to 9.0×10^{-8} are shown in Figs. 7(b)−(d), respectively. In Fig. 7(b), clearly, the growth exponent increases with increasing the strain rate, which may cause the coalescence of the voids in the later stage of evolutionary process and consequently result in formation of a large number of cracks. While in Figs. 7(c) and (d), with increasing the strain rate, the growth exponent increases initially (i.e., from 0.669 to 0.766 and from 0.653 to 0.665, respectively) and then decreases

(i.e., from 0.766 to 0.637 and from 0.665 to 0.651, respectively). In early stage of the evolutionary process, the deformation promotes the nucleation and growth of Kirkendall voids by providing more atomic mismatch regions and vacancies as also indicated in Ref. [18]. In later stage of the evolutionary process, the growth exponent decreases due to the lack of vacancies which are not sufficient for growth of the voids. The values of the growth exponent, which lie in the range of 0.6−1.0, indicate that the nucleation of Kirkendall voids takes place at the interface [27].

However, it is worth noting that there are effects of the cyclic strain rate on the growth exponent of Kirkendall voids. When the strain rate is equal to or greater than 1.0×10^{-6}, both of the average size and growth exponent of Kirkendall voids increase with increasing the strain rate. The large strain rate ($\dot{\varepsilon}\geq7.0\times10^{-6}$) can cause the coalescence of the voids in the later stage of the evolutionary process. The growth rate of Kirkendall voids increases rapidly with increasing the growth exponent. When the strain rate is equal to or smaller than 9.0×10^{-7}, with increasing the strain rate, the size of the voids increases monotonically, while the growth exponent increases initially and then decreases.

3.3 Evolution of Kirkendall voids with different lengths of cyclic period

Figure 8 shows the morphological evolution of Kirkendall voids with different lengths of cyclic period for 200, 1000 and 5000 time steps, respectively, with different evolutionary time elapsed from 1.0×10^5 to 3.0×10^5 and then to 7.0×10^5. The way of applying the constant cyclic strain rate (6.0×10^{-6}) is explained briefly as follows: for instance, the length of the cyclic for 200 time steps means that the strain rate is applied along the interface during the first 100 time steps and the same constant strain rate is employed in the opposite direction during 101−200 time steps. The same way was used for the cyclic period with length of 1000 and 5000 time steps. It can be seen clearly in Fig. 8 that Kirkendall voids nucleate preferentially at the interface in the initial stage of the evolutionary process, and the coalescence of the voids cannot be seen clearly in the later stage of the evolutionary process. The atomic mismatch regions at the interface, as shown in Figs. 8(a_1), (b_1) and (c_1), promote the nucleation of Kirkendall voids with decreasing the interface energy.

The changes of the average size of Kirkendall voids versus evolutionary time with different lengths of cyclic period (i.e., 200, 500 and 5000 time steps, respectively) and the growth exponent of Kirkendall voids versus the length of cyclic period are shown in Fig. 9. Apparently, the average size of Kirkendall voids increases with increasing the evolutionary time, as shown in Fig. 9(a). There is only a small effect on the average size of Kirkendall void when changing the length of the cyclic period from 200 to 500 and then to 5000. Notably, in Fig. 9(b), the trend of the growth exponent of Kirkendall voids changing with the length of cyclic period (herein, six values are counted, i.e., T_L=200, 300, 500, 1000, 2000 and 5000) shows an initial increase (from 0.764 to 0.812) and then a gradual decrease (from 0.812 to 0.726), indicating that the length of cyclic period in the same evolutionary process has a significant influence on the growth exponent of the voids. According to the classical theory of transformations in metals and alloys [27], the grain boundary nucleation after saturation occurs when the growth exponent is less than 1, while the grain edge nucleation after saturation takes place with the growth exponent value between 1 and 2. The values of the growth exponent, which lie in the range of 0.726−0.812, indicate that the nucleation of Kirkendall voids occurs at the interface [27]. Thus, as shown in simulation results of the present study, the change in the length of cyclic period has no large influence on the nucleation site of the voids. When changing the length of cyclic period, there

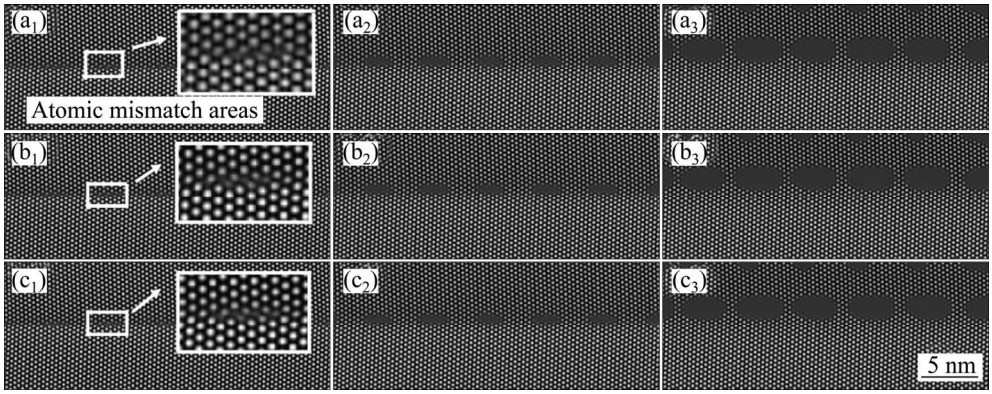

Fig. 8 Morphological evolution of Kirkendall voids with different lengths of cyclic period of T_L=200 time steps (a_1−a_3), T_L=1000 time steps (b_1−b_3) and T_L=5000 time steps (c_1−c_3), and different evolutionary time of t=1.0×10^5 (a_1−c_1), t=3.0×10^5 (a_2−c_2) and t=7.0×10^5 (a_3−c_3)

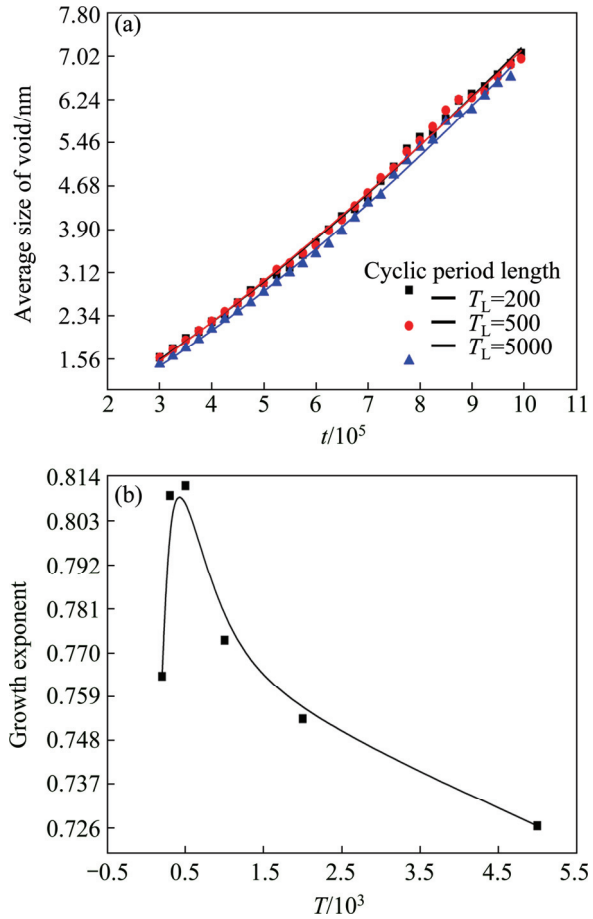

Fig. 9 Changes of average size of Kirkendall voids vs time under different lengths of cyclic period (a) and growth exponent of Kirkendall voids vs length of cyclic period (b)

is only a small effect on the average size of the voids but a significant effect on the growth exponent.

4 Conclusions

1) Under three different deformation conditions, i.e., a constant strain rate, an alternating tensile−compressive square-wave form strain rate and a square-wave form constant strain rate with different lengths of the period applied along the interface, Kirkendall voids nucleate preferentially at the interface, and the average size of the voids increases with the time and strain rate.

2) Under a constant strain rate applied along the interface, in the evolutionary process the coalescence growth of Kirkendall voids is not apparent, while there is an obvious coalescence of the voids in the later stage of the evolutionary process under a large strain rate ($\dot{\varepsilon} \geq 7.0\times10^{-6}$).

3) Under an alternating tensile−compressive square-wave form strain rate applied along the interface, Kirkendall voids grow parallel to the interface. When the strain rate is equal to or greater than 1.0×10^{-6}, the growth exponent increases with the strain rate, which may cause the coalescence of the voids in the later stage of evolutionary process and consequently result in formation of cracks. When the strain rate is equal to or smaller than 9.0×10^{-7}, with increasing the strain rate, the growth exponent increases initially and then decreases.

4) Under a square-wave form constant strain rate with different lengths of the cycle period applied along the interface, there is only little effect on the average size of the voids but a significant influence on the growth exponent when changing the length of the cyclic period. With increasing the length of the cycle period, the growth exponent increases at first and then decreases.

References

[1] KE Chang-bo, ZHOU Min-bo, ZHANG Xin-ping. Phase field simulation on microstructure evolution and growth kinetics of Cu_6Sn_5 intermetallic compound during early interfacial reaction in Sn/Cu soldering system [J]. Acta Metallurgica Sinica, 2014, 50(3): 294−304. (in Chinese)

[2] ZHOU Min-bo, MA Xiao, ZHANG Xin-ping. Undercooling behavior and intermetallic compound coalescence in microscale Sn−3.0Ag−0.5Cu solder balls and Sn−3.0Ag−0.5Cu/Cu joints [J]. Journal of Electronic Materials, 2012, 41(11): 3169−3178.

[3] YUE Wu, QIN Hong-bo, ZHOU Min-bo, MA Xiao, ZHANG Xin-ping. Electromigration induced microstructure evolution and damage in asymmetric Cu/Sn−58Bi/Cu solder interconnect under current stressing [J]. Transactions of Nonferrous Metals Society of China, 2014, 24(5): 1619−1628.

[4] ZHAO Ning, ZHONG Yi, HUANG Ming-liang, MA Hai-tao. Research progress in thermomigration of metal atoms in micro solder joints and its effect on interfacial reaction [J]. The Chinese Journal of Nonferrous Metals, 2015, 25(8): 2157−2166. (in Chinese)

[5] LI Xue-mei, SUN Feng-lian, ZHANG Hao, XIN Tong. Effect of temperature on interface diffusion in micro solder joint under current stressing [J]. Transactions of Nonferrous Metals Society of China, 2015, 25(5): 1699−1703.

[6] JU Guo-kui, WEI Xi-cheng, SUN Peng, LIU Jian-ying. Effects of interfacial IMC on tensile fracture behavior of Sn−3.0Ag−0.5Cu solder joints on copper substrates [J]. The Chinese Journal of Nonferrous Metals, 2007, 17(12): 1936−1942. (in Chinese)

[7] MA Wen-jing, KE Chang-bo, ZHOU Min-bo, LIANG Shui-bao, ZHANG Xin-ping. Phase field crystal simulation on evolution and growth kinetics of Kirkendall voids in interface and intermetallic compound layer in Sn/Cu soldering system [J]. Acta Metallurgica Sinica, 2015, 51(7): 873−882. (in Chinese)

[8] MURALI S, SRIKANTH N, VATH C J. Effect of wire size on the formation of intermetallics and Kirkendall voids on thermal aging of thermosonic wire bonds [J]. Materials Letters, 2004, 58(25): 3096−3101.

[9] ANGENETE J, STILLER K. Oxidation of simple and Pt-modified aluminide diffusion coatings on Ni-base superalloys−II. Oxide scale failure [J]. Oxidation of Metals, 2003, 60(1−2): 83−101.

[10] KAGANOVSKII Y S, PARITSKAYA L N, BOGDANOV V V. Lateral propagation of intermetallic phases in coarse and nano-grained Cu/Sn diffusion couples [J]. Powder Metallurgy and Metal Ceramics, 2008, 47(11−12): 652−659.

[11] JUNG Y, YU J. Electromigration induced Kirkendall void growth in Sn−3.5Ag/Cu solder joints [J]. Journal of Applied Physics, 2014, 115(8): 083708.

[12] YANG X J, CHOW C L, LAU K J. Time-dependent cyclic

deformation and failure of 63Sn/37Pb solder alloy [J]. International Journal of Fatigue, 2003, 25(6): 533−546.
[13] YU H C, van der VEN A, THORNTON K. Theory of grain boundary diffusion induced by the Kirkendall effect [J]. Applied Physics Letters, 2008, 93(9): 091908.
[14] BELYAKOV S, ATKINSON H V, GILL S P A. Crystallographically faceted void formation in the matrix of lead-free solder joints [J]. Journal of Electronic Materials, 2010, 39(8): 1295−1297.
[15] MÜLLER W H, WEINBERG K, BÖHME T. On the effect of Kirkendall voids on solder joint reliability [J]. Proceedings in Applied Mathematics and Mechanics, 2007, 7(1): 4030035−4030036.
[16] ZENG K J, STIERMAN R, CHIU T C, EDWARDS D, ANO K, TU K N. Kirkendall void formation in eutectic SnPb solder joints on bare Cu and its effect on joint reliability [J]. Journal of Applied Physics, 2005, 97(2): 024508.
[17] KIM D, CHANG J H, PARK J, PAK J J. Formation and behavior of Kirkendall voids within intermetallic layers of solder joints [J]. Journal of Materials Science: Materials in Electronics, 2011, 22(7): 703−716.
[18] WEINBERG K, BÖHME T, MÜLLER W H. Kirkendall voids in the intermetallic layers of solder joints in MEMS [J]. Computational Materials Science, 2009, 45(3): 827−831.
[19] ELDER K R, PROVATAS N, BERRY J, STEFANOVIC P, GRANT M. Phase-field crystal modeling and classical density functional theory of freezing [J]. Physical Review B, 2007, 75(6): 064107.
[20] ELDER K R, THORNTON K, HOYT J J. The Kirkendall effect in the phase field crystal model [J]. Philosophical Magazine, 2011, 91(1): 151−164.
[21] BERRY J, ELDER K R, GRANT M. Melting at dislocations and grain boundaries: A phase field crystal study [J]. Physical Review B, 2008, 77(22): 224114.
[22] HIROUCHI T, TAKAKI T, TOMITA Y. Development of numerical scheme for phase field crystal deformation simulation [J]. Computational Materials Science, 2009, 44(4): 1192−1197.
[23] ELDER K R, GRANT M. Modeling elastic and plastic deformations in nonequilibrium processing using phase field crystals [J]. Physical Review E, 2004, 70(5): 051605.
[24] OONO Y, PURI S. Study of phase-separation dynamics by use of cell dynamical systems. I. Modeling [J]. Physical Review A, 1988, 38(1): 434−453.
[25] KIM B J, LIM G T, KIM J, LEE K, PARK Y B, JOO Y C. Intermetallic compound and Kirkendall void growth in Cu pillar bump during annealing and current stressing [C]//Proceeding of 58th Electronic Components and Technology Conference. Orlando, Florida, USA: IEEE, 2008: 336−340.
[26] CHAO B, CHAE S H, ZHANG X F, LU K H, DING M, IM J, HO P S. Electromigration enhanced intermetallic growth and void formation in Pb-free solder joints [J]. Journal of Applied Physics, 2006, 100(8): 084909.
[27] CHRISTIAN J W. The theory of transformations in metals and alloys [M]. London: Pergamon Press Oxford, 2002.

二元合金体系形变过程中 Kirkendall 空洞形貌演化和生长动力学的晶体相场法研究

马文婧，柯常波，梁水保，周敏波，张新平

华南理工大学 材料科学与工程学院，广州 510640

摘　要：采用晶体相场法研究了二元合金形变过程中界面 Kirkendall 空洞的形貌演化和生长过程。研究表明，Kirkendall 空洞优先在界面处形核，空洞尺寸随着演化时间和应变速率的增加而增大。在恒定和循环应变速率较大时，空洞发生明显的合并生长。当循环应变速率大于 1.0×10^{-6} 时，空洞生长指数随应变速率的增加而增大；当循环应变速率小于 9.0×10^{-7} 时，空洞生长指数随着应变速率的增加呈先增大后减小的变化规律。在相同的循环应变速率不同循环周期长度情况下，空洞生长指数随着循环周期长度的增加呈先增大后减小的变化规律。

关键词：Kirkendall 空洞；二元合金；晶体相场方法；生长指数；形变

(Edited by Xiang-qun LI)